Scaling ice-induced vibrations by combining replica modeling and preservation of kinematics

Hammer, Tim C.; Puolakka, Otto; Hendrikse, Hayo

DOI
10.1016/j.coldregions.2024.104127

Publication date
2024

Document Version
Final published version

Published in
Cold Regions Science and Technology

Cold Regions Science and Technology 220 (2024) 104127

Contents lists available at ScienceDirect

Cold Regions Science and Technology

journal homepage: www.elsevier.com/locate/coldregions

Scaling ice-induced vibrations by combining replica modeling and preservation of kinematics

Tim C. Hammer [a,*], Otto Puolakka [b], Hayo Hendrikse [a]

[a] Delft University of Technology, Faculty of Civil Engineering and Geosciences, Department of Hydraulic Engineering, Stevinweg 1, 2628 CN Delft, the Netherlands
[b] Aalto University, School of Engineering, Department of Mechanical Engineering, P.O. Box 14300, FI 00076 Aalto, Finland

ARTICLE INFO

Keywords:
Ice tank experiments
Model tests
Hybrid test setup
Crushing
Offshore structures

ABSTRACT

A modeling approach to simulate ice-induced vibrations of vertically sided offshore structures in ice tank experiments is presented. The technique combines replica modeling with the preservation of kinematics during ice-structure interaction. The technique was chosen based on the theoretical understanding that ice-induced vibrations are caused by an energy exchange between the structure and the ice. The mechanism is controlled by primarily four aspects: the kinematics during ice-structure interaction, the degree to which the ice can resist higher loading at low velocities prior to failure (velocity effect), the existence of a transition speed from ductile-to-brittle failure, and the mean ice load level.

A model ice type which resulted in a velocity effect and provided a transition speed comparable to that of sea ice was developed and used during ice tank experiments. A scaling factor, derived from the comparison between the mean brittle crushing ice load of the full-scale event and the in-situ measured mean brittle crushing model ice load, was applied to scale structure properties of a numerical model. This model was implemented during real-time hybrid simulations in model ice to preserve kinematics during the ice-structure interaction.

To verify the proposed scaling approach, rigid indenter experiments covering velocities from 0.1 mm s^{-1} to 500 mm s^{-1} and dynamic ice-induced vibration experiments of structures with varying aspect ratios (8 and 12) and shapes (cylindrical and rectangular) were conducted. Neither the aspect ratio nor shape appeared to influence the development of ice-induced vibrations significantly.

The approach was qualitatively validated by reproducing full-scale ice-induced vibrations as experienced by the Molikpaq platform and Norströmsgrund lighthouse.

1. Introduction

Recordings of ice-induced vibrations of vertically sided offshore structures are rare, leading to insufficient data for detailed theoretical developments. To address this gap, ice tank tests have been conducted over the last decades to explore the mechanisms governing ice-structure interaction of (near-)vertically sided structures (Määttänen, 1979; Toyama et al., 1983; Kärnä and Muhonen, 1990; Sodhi, 1991; Kärnä et al., 2003; Yue et al., 2006; Huang et al., 2007; Määttänen et al., 2012; Hendrikse et al., 2018). A further use of ice tank tests is to investigate the potential for ice-induced vibrations of completely new structures to be built in locations with sea ice presence, such as done for offshore wind turbines (Barker et al., 2005; Gravesen et al., 2005; Tian et al., 2019), lighthouses (Määttänen, 1978) or offshore oil- and gas platforms (Timco et al., 1992; Cornett and Timco, 1998; Sodhi, 2001). Many of the conducted experiments were scaled for a combination of Froude and Cauchy scaling, which resulted in challenges to achieve ice failure modes and structural responses representative of full-scale events.

The Cauchy scaling method considers a strength value related to an elastic force component, based on the Young's modulus of the ice (e.g., elastic control factor by Huang et al. (2007)). However, as both saline and freshwater ice exhibit non-elastic behavior under loading scenarios relevant for ice-induced vibrations (Cole and Durell, 1995; Wei et al., 2022; Owen et al., 2023), the adequacy of considering only an elastic force component is questionable. Yap (2011) also emphasized that "strength is a function of several known [and unknown] factors" and von Bock und Polach and Molyneux (2017) pointed out that corresponding relative speeds during ice-structure interaction on vertically sided offshore structures "may be in the ductile region, which again presents a challenge for model basins, as Froude-Cauchy scaling does not apply, as

* Corresponding author.
E-mail address: t.c.hammer@tudelft.nl (T.C. Hammer).

https://doi.org/10.1016/j.coldregions.2024.104127
Received 12 October 2023; Received in revised form 11 December 2023; Accepted 12 January 2024
Available online 19 January 2024

strain rate scales under [such] system[s]."

Sodhi (1992) noted during indentation tests with freshwater ice that effective pressures measured on small and large structures were similar when indentation velocities were kept unscaled. Kamesaki et al. (1996) introduced the dimensionless compliance effect to scale ice-induced vibrations. A recent insight is that the observed compliance effect can be explained by the (relative) velocity effect between structure and ice (Owen et al., 2023).

Additionally, full-scale events of ice-induced vibrations indicate that the ice load level is dependent on the relative velocity between the structure and the ice. For example, measurements at the Molikpaq platform (Jefferies and Wright, 1988) or at a beam attached to one leg of a drilling platform in the Cook Inlet (Peyton, 1968) showed that the crushing ice load level increased when the ice slowed down during the interaction.

Sodhi (1992) suggested using replica modeling for investigating ice-structure interaction in reduced-scale experiments. In replica modeling, the geometric scale is maintained, and identical materials are used at corresponding locations (Baker et al., 1991). Consequently, the effective mean pressure at the ice-structure interface is preserved. Building upon the study by Sodhi (1992), Yap (2011) applied replica modeling and scaled time and structural displacement amplitude with the same geometrical scaling factor, utilizing the Cauchy scaling.

Ziemer (2021) preserved time in model-scale experiments assuming that the strain rate governs ice-induced vibrations of vertically sided structures. Ziemer (2021) only scaled the structural displacement amplitude, assuming length-independent ice failure. However, Ziemer's conclusion favored velocity preservation over strain rate preservation to achieve representative ice-induced vibrations. This would require adjusting structural stiffness to compensate for differences in the crushing load between model and offshore structures, potentially leading to large geometric scales in ice tank experiments.

Ice-induced vibrations are primarily controlled by the energy transfer between ice and structure which is mainly, from the ice perspective, defined by the magnitude of the ice forces on the structure. Furthermore, the magnitude of the ice forces during interaction has been shown to be strongly dependent on the relative velocity between ice and structure. At low relative velocities larger forces are observed, which is referred to as the velocity effect (Izumiyama et al., 1994; Jefferies et al., 2008; Kamesaki et al., 1996; Kärnä et al., 2008; Määttänen, 1981; Owen et al., 2023; Singh et al., 1990; Sodhi, 2001; Tsuchiya et al., 1985). This effect is also observed on completely rigid structures, for which the relative velocity becomes just the ice drift speed, where the largest global forces are typically obtained at a transition velocity (e.g., Takeuchi et al., 2001). This transition velocity is here referred to as the velocity at which the global failure behavior of the ice changes from creep to crushing, or the ductile-to-brittle transition velocity. This transition velocity, and the associated high ice forces when compared to the forces for indentation velocities far exceeding the transition, are key properties of the ice, which control, together with the mean load level, the absolute possible energy transfer and the rate of energy transfer to the structure during interaction. If these model ice properties can be kept within similar ranges as observed in sea ice, full-scale ice-induced vibration events in model ice experiments could be reproduced.

For this purpose, a replica modeling technique with a preservation of kinematics during the ice-structure interaction is applied, in line with suggestions from literature (i.e., Sodhi, 1992). Contrary to other scaling methods, this scaling method underlines that it is unknown how to scale the time- and rate-dependent behavior of ice, or how to scale the amplitude of structural oscillation without affecting the development of ice-induced vibrations in an uncontrolled manner, which is why a preservation of the kinematics is applied.

Similarity of structure shape, aspect ratio, Young's modulus, compressive strength, ice mass, local peak pressure at high speed (i.e., brittle crushing peak loads), surface friction, and ice temperature are assumed to not be required to achieve representative ice-induced vibration in model ice experiments.

The following chapter first defines how such representative ice-induced vibrations are defined in the present study. Then it introduces how the replica modeling and preservation of kinematics were assured in model ice experiments and summarizes the applied scaling factors. Chapter 3 introduces the cold model ice developed for the model ice experiments, with a focus on the transition velocity and the velocity effect. In Chapter 4, the significance of the structure shape and aspect ratio between structure diameter and ice thickness on the velocity effect, transition speed, and development of ice-induced vibrations are investigated. Results from scaled model experiments aiming at specific full-scale events from the Norströmsgrund lighthouse and Molikpaq are presented in Chapter 5 for a qualitative validation of the applied method.

2. Methodology

A representative scaled test for ice-induced vibrations is further defined as a test in which the regimes of ice-induced vibrations (i.e., frequency lock-in and intermittent crushing) develop as observed during full-scale ice-induced vibration events or other reference data with their characteristics preserved (e.g., Hendrikse and Nord, 2019; Hammer et al., 2022), and with global loads and structural kinematics qualitatively similar to those of full-scale ice-induced vibration events. A key characteristic is that an ice floe slowing down against a relatively flexible structure can cause a transition from continuous brittle crushing to frequency lock-in and ultimately to intermittent crushing (Jefferies and Wright, 1988; Peyton, 1968). Here the relative increase in global peak loads, as intermittent crushing develops, should be captured, as well as the increase in period of the saw-teeth as the ice drift speed decreases. Experience showed the two latter aspects to not develop in 'standard' model-ice, most likely due to the tendency of the ice to bend or buckle under high loading (Hendrikse et al., 2018).

2.1. Replica modeling

Replica modeling uses a model dimensionally identical to the full-scale structure, with identical materials placed at corresponding geometric positions (Baker et al., 1991).

This approach can be understood as preserving the effective mean ice pressure as shown by conducted experiments (Sodhi, 1992) and application in scaling (Yap, 2011). If the mechanism(s) causing ice-induced vibrations originate at a small scale in the ice (Hendrikse and Nord, 2019; Cole, 2021), then the finding of Sodhi (1992) seems to be reasonable when the specimen is much larger than the ice grain size. We assume that the effective mean pressure preservation is achievable when the ratio of structural diameter (D) to grain size (D_{gr}) is relatively large: $\frac{D}{D_{gr}} > 25$ (Hirayama et al., 1974) and only when testing at mass-unaffected velocities.

2.2. Preservation of kinematics during dynamic ice-structure interaction

Literature indicates that neither the structural displacement amplitude nor time should be scaled, which leads to a preservation of the kinematics during the dynamic ice-structure interaction. Here preservation is defined as a state in which physical quantities are kept at the full-scale value. To preserve kinematics during interaction, properties of the ice *and* of the offshore structure must therefore be kept at full-scale (see properties listed in Table 2).

2.2.1. Ice

The transition speed from ductile-to-brittle ice failure and the velocity effect are central to the development and scaling of ice-induced vibrations of vertically sided structures (Hendrikse and Nord, 2019). The model ice was therefore required to have a similar transition speed

and show a similar velocity effect as sea ice. The transition from ductile-to-brittle crushing was identified as the ice drift speed that led to the highest standard deviation of the global ice load in rigid indenter experiments of sufficient duration. This definition aligns with Takeuchi et al. (2001), who determined the transition speed by visually confirming reduced prominence of low-frequency load peaks in the signal. The standard deviation was chosen as a classification criterion as it considers the change of load peak prominence when no mass effects (i.e., ice extrusion) are influencing the mean load.

2.2.2. Structure

A real-time hybrid test setup (Fig. 1) was used in the experiments to achieve full-scale kinematics of the offshore structure during ice-structure interaction. A hybrid test setup is based on a substructuring technique. Typical setups for dynamic testing are divided into two parts using a substructuring technique, as described by McCrum and Williams (2016): "[C]ritical structural subassemblies that are fundamental to the overall response of the structure are physically tested, whilst the remainder of the structure whose response can be more easily predicted is numerically modelled."

In our case, the real-time hybrid test setup consists of a physical substructure, equipped with ice load measurement devices, and a numerical substructure comprising a numerical model for predicting the structural response of offshore structures and a servo controller for controlling the transfer system (i.e., electrical actuators). The real-time hybrid test setup helps to preserve relative velocity, without requiring large structure models in the ice tank. Before testing, a numerical structure model (e.g., a file containing scaled structural properties of a specific offshore structure) was uploaded to the numerical model. As the physical substructure was moved through the ice sheet, the measured ice load was used as input for the numerical model. The numerical model solved the dynamic equations in real time using a Euler-Cromer method to determine the structural displacement of the offshore structure, which was then applied on the physical substructure by an electrical actuator. The application of a hybrid test setup led to a "decoupling" between oscillation and substructure, as suggested by Ziemer (2021).

The hybrid test setup employed is a modified version of the system used during the first experimental model test campaign of the SHIVER project in 2021 (Hendrikse et al., 2022). Additional details about the measurement systems, a flow diagram of the hybrid test setup, and verification of the structural simulation method can be found in Hammer et al. (2021). The current study used a different ice load measurement system to avoid temperature-induced strain issues (Hammer and Hendrikse, 2023).

Instead of using strain gauge rings, three separate load cells (2960–2962-2965 low-profile (pancake) load cells SENSY S.A, 6040 Jumet, Belgium) were positioned between the aluminum pile and the moving tables (Fig. 1 - right) to determine the ice-induced bending moments. For the tests with vertically sided indenters, the vertical load component was disregarded when calculating horizontal ice loads, as these were small relative to the horizontal loads (see Figure 1 in the supplementary material). The static arms of load application point to the load cells and a sketch of this scenario are given in Figure 2 and Table 4 in the supplementary material.

Additionally, the aluminum test pile was shortened to accommodate the connection of red 3D-printed adapters (Fig. 1 - left), which allowed investigation of geometrical scale effects using different shape and diameter indenters without increasing the mass of the physical substructure or increasing manufacturing cost and time significantly. The suitability of using 3D-printed structures made of polylactic acid for model tests of vertically sided structures in model ice was explored by Petry et al. (2023). To minimize the risk of local damage, selective laser sintering (SLS) of polyamide 12 was favored over the tested fused deposition modeling technique used in Petry et al. (2023). Material similarity of the physical substructure (consisting of aluminum or polyamide 12) and the offshore structures (constructed from steel or concrete) was assumed when assessing the crushing of ice against a vertical interface. This means that neither material used in the experiments yields significantly, which would on the one hand change the relative velocity between structure and ice and on the other hand affect the hybrid test setup control. Both the aluminum and 3D prints were designed so that the deformation under maximum loading was negligible. After manufacturing, the SLS-prints were painted red to enhance better visual contrast with the crushing ice. Tested substructures can be seen in Fig. 2 and further specifications of the substructures can be found in Table 1.

2.3. Scaling factors

While simulating and preserving the global ice drift speed is feasible by moving a structure with the full-scale speed through the model ice, maintaining structural kinematics is more complex. To address this challenge, a real-time hybrid setup was employed, enabling the scaling of structural properties in a numerical domain while testing a "decoupled" physical substructure in an ice tank. Assuming mean pressure preservation, the structural properties of the full-scale structure (e.g., mass, damping, and stiffness) were scaled to account for the difference in the loaded area between full- and model-scale. A scale factor λ_F between the measured quasi-static mean ice load measured on the physical substructure in model ice experiments ($\overline{F}_m$) and the quasi-static mean ice load of the full-scale event ($\overline{F}_f$) was applied to scale the structural properties in the numerical model implemented in the real-time hybrid simulations:

$$\lambda_F = \frac{\overline{F}_f}{\overline{F}_m}. \tag{1}$$

The model ice load $\overline{F}_m$ was determined through an ice load measurement from a rigid indenter test at an ice drift speed of 100 mm s^{-1} for a 1.5 m crushing length at the start of each separate test run through the ice sheet. Note that the controlled indenter speed (carriage speed) is interpreted as ice drift speed in the present study. The value of 100 mm s^{-1} was chosen to reflect the upper bound of rate-independent mean

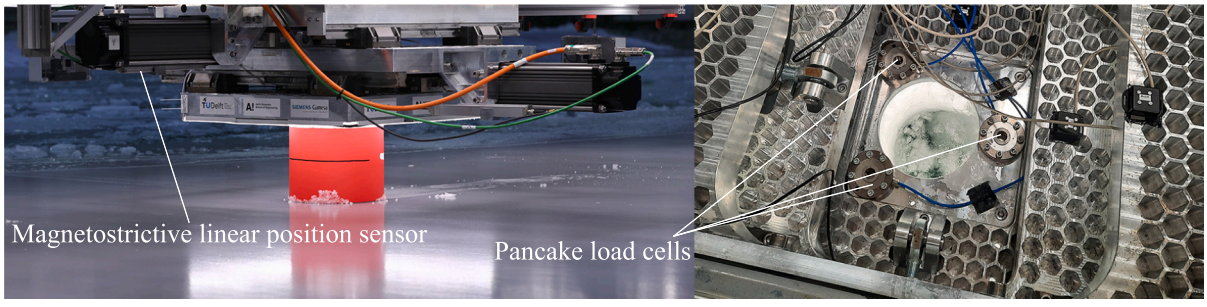

Fig. 1. Left: Physical substructure and transfer system of the real-time hybrid test setup. Right: Top view on the pancake load cells once the aluminum pile was removed.

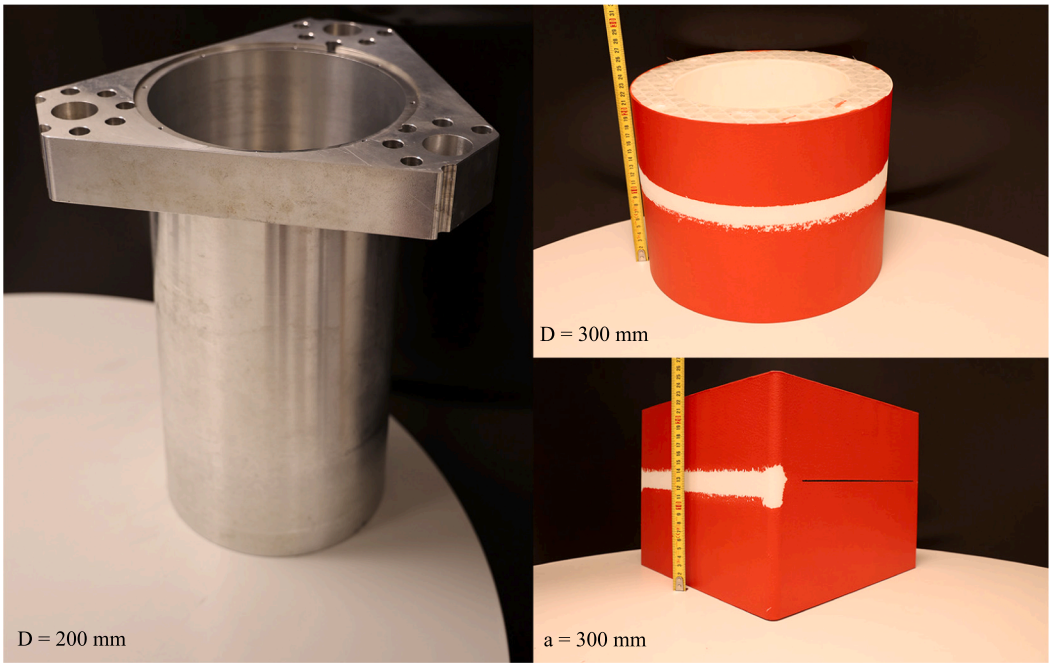

Fig. 2. Left: Aluminum pile. Top right: Cylindrical (C) SLS-print. Bottom right: Rectangular (R) SLS-print.

Table 1
Specification of investigated physical substructures.

Structure	Material	D (a)	Height	Aspect ratio	Application	Technical drawings
[−]	[−]	[mm]	[mm]	[−]	[−]	[−]
Pile	Aluminum	200	378	8	Rigid, Molikpaq, NSG lighthouse	see supplementary material
SLS-C	Polyamide 12	300	230	12	Rigid	see supplementary material
SLS-R	Polyamide 12	(300)	230	12	Rigid	see supplementary material

pressures as found by Sodhi (1992). Mean ice loads as measured during rigid indenter experiments in four model ice sheets are shown in Fig. 3. The chosen speed (100 mm s^{-1}) is at the upper limit of ice drift speeds resulting in minor rate effects (grey area). The boundaries of the grey area are set for ice drift speeds that did not exceed a median load variation of ±15% when compared to the chosen median load as measured for an ice drift speed of 100 mm s^{-1}.

The full-scale mean load $\overline{F}_f$ can be extracted from project reports, estimated by design guidelines, or be simulated with ice models coupled to rigid structures (see Section 6.4). A summary of the applied scaling factors is provided in Table 2.

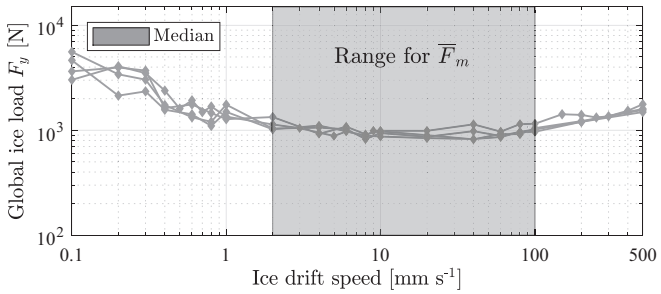

Fig. 3. Global ice loads measured during rigid indenter experiments in four model ice sheets.

3. Model ice

3.1. Cold model ice

Model ice experiments were conducted in the Ice and Wave tank of Aalto University in Espoo, Finland. The model ice used in the present study was produced by spraying a fine mist through water nozzles in 60 cycles at an air temperature of −10.5 °C, following the growth of an initial carrying ice layer for 20 min. Using a spraying speed of 0.16 m s^{-1}, the total spraying time was 225 min. Subsequently, the ice underwent 150 freezing degree hours at a constant temperature of −12 °C. The ice was maintained at −11 °C during testing. This ice type is henceforth referred to as cold model ice. The experiments were conducted with a sprayed ice thickness of 25 mm. The reader is referred to Figs. 4 and 5 of Hendrikse et al. (2022) to find vertical cross-sections, and thin sections of the resulting model ice. Facilities for thin sectioning were unavailable at the time of the present experiments. The grain size in these figures is visually estimated to be in the order of 1 mm. For comparison, von Bock und Polach et al. (2013) defined the highest probable grain size as 0.68 mm for ethanol-doped model ice in the same Ice and Wave tank, using the same spraying nozzles.

3.2. Ductile-to-brittle transition speed and velocity effect

Results of rigid indenter tests in the cold model ice are shown in Fig. 4. The cold model ice manages to resist increased load levels at lowest ice drift speeds (velocity effect). A transition speed of 0.1 mm s^{-1} is identified for the cold model ice. It should be noted that the value could theoretically be lower as the standard deviation was highest for the lowest ice speed tested. However, it can be assumed that the

Table 2
Scale factors based on the scale factor λ_F.

Physical quantity	Unit	Scale factor applied
General		
Length*	[m]	1
Time	[s]	1
Structure		
Frequency	[s^{-1}]	1
Damping ratio	[−]	1
Mass-normalized mode shape	[$kg^{-0.5}$]	$\lambda_F^{-0.5}$
Mass	[kg]	λ_F
Stiffness	[N m^{-1}]	λ_F
Damping	[Ns m^{-1}]	λ_F
Ice		
Ice drift speed	[m s^{-1}]	1
Mass	[kg]	~1 at micro scale
Mean brittle crushing force**	[N]	λ_F
Transition speed from ductile-to-brittle failure	[m s^{-1}]	~1 (discussed in Section 3.2)
Strength	[N m^{-2}]	<1 (discussed in Section 3.3)
Thickness	[m]	Section 4.1
Aspect ratio	[−]	Section 4.1

* The length scaling applies to response not to geometry.
** Determined for a crushing length of 1.5 m at an ice drift speed of 100 mm s^{-1} as described above.

transition speed is almost reached as a levelling trend for lowest tested ice drift speed can be observed.

The cold model ice exhibits similar transition speeds as sea ice, comparing the identified transition speed to those observed in sea ice 'close' to the location of the full-scale scenarios (0.08–0.17 mm s^{-1} - Table 3) or of freshwater ice in the lab (0.06–0.11 mm s^{-1} (Wu et al., 1976)).

3.3. Standard scaling parameters

Although not considered in the scaling, Young's modulus and compressive strength were tested and put into relation with full-scale data, as they are standard parameters and analysis creates a better comparability to existing scaling methods and ice types.

Compressive in-situ strength tests, flexural in-situ strength tests, and Young's modulus measurements were conducted at least once a day for the cold model ice in accordance with the ITTC guideline (2021). Comparison of field measurements (Table 3) with material properties as measured in the ice tank (Table 4) reveals that the compression strength σ_c of the cold model ice, although being relatively high, is still lower than the compressive strength of sea ice. Similarly, the Young's modulus E of the cold model ice, although being relatively high, is lower than measured values in sea ice.

It is important to put this result into perspective. To our knowledge, no ice property measurements exist for the dates of full-scale events which we aimed to simulate in the ice tank. Properties from similar locations and times were extrapolated to the investigated cases which increases uncertainty in the comparison. But most importantly, achieving elastic similarity is of secondary interest in the present study, as the primary concern is to preserve kinematics. Furthermore, strength tests in model scale are complex, as pressure-area, geometry, grain size, and stress functions may form co-dependencies (von Bock und Polach and Ehlers, 2015).

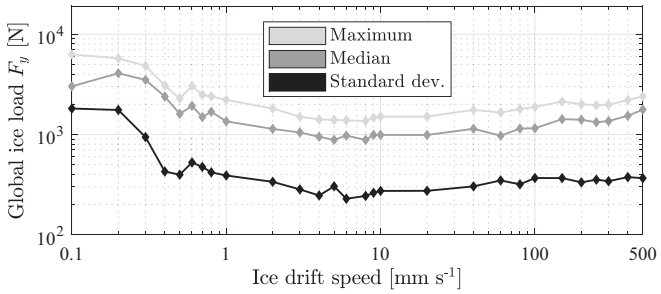

Fig. 4. Ice loads from rigid indenter tests for cold model ice. Rigid experiments were performed with an aluminum pile (D = 200 mm) and an ice thickness of 25 mm.

4. Scaling effects

Next it is investigated if the assumption to neglect similarity of structure shape and aspect ratio when scaling for ice-induced vibrations can be verified. Rigid indenter and dynamic ice-induced vibration experiments of structures with two different aspect ratios and structure shape have been conducted and analyzed.

4.1. Aspect ratio

Experimental results of rigid indenter tests for substructures with two different diameters are shown in Fig. 5. Changing from a smaller to a larger diameter had no discernible effect on the transition speed or velocity effect. The ratios between the standard deviation and median ice load remained similar for both tested substructures. Notably, these substructures both exhibited a slightly increasing ratio for low ice drift speeds, and a decreasing ratio for higher ice drift speeds. This trend was more pronounced with increased structural diameter. This observation might be associated with the ice failure type. Typically, two ice failure types are distinct: at a high relative velocity between structure and ice, the ice fails randomly and non-simultaneously in time and space along the structural surface, often related to local peak load generation and small contact area. At a low relative velocity, the ice fails simultaneously, synchronized in time and space along the surface of the structure, which often leads to higher global load peak loads and increased contact area. For non-simultaneous ice failures, the averaging of random processes over a larger area led to a reduction in the ratio. In cases of ice drift speeds corresponding to simultaneous ice failure, the increased area appeared to enhance the likelihood of simultaneous loading and consequent global load peak generation. Extrapolating this finding to full-scale dimensions, an increased standard deviation for experimental data can be expected when compared to full-scale data. However, this effect is negligible here as the suggested scaling method is based on the central tendency of the brittle crushing load and not on the peak pressures.

Investigating the effect of a change in the aspect ratio on the development of ice-induced vibrations, dynamic ice-induced vibration experiments of structures with two different aspect ratios were conducted in the cold model ice. The comparison of time series of four

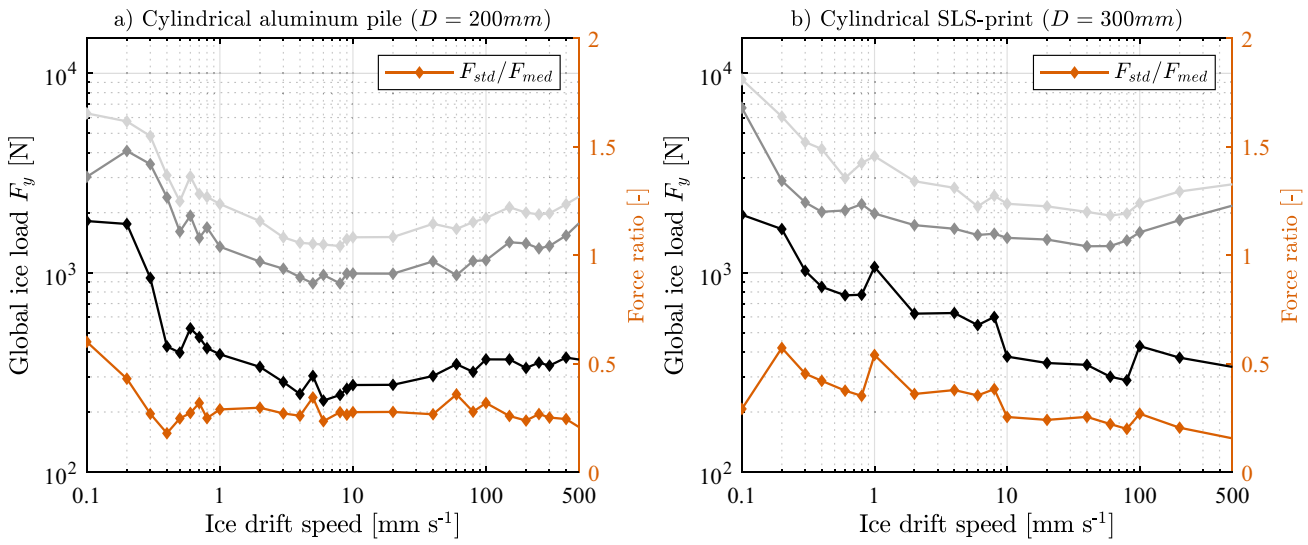

Fig. 5. Statistical measures derived by rigid indenter tests for structures of similar shape but different diameter.

Table 3
Examples of mechanical sea ice properties. The transition speed v_t is based on the strain rate that resulted in the maximum uniaxial compression strength.

Ice Type	Location	T	v_t	σ_c	E	σ_f	D_{gr}	Reference
[−]	[−]	[°C]	[mm s^{-1}]	[MPa]	[GPa]	[kPa]	[mm]	
Sea ice floe	Bay near the NSG lighthouse	-1	0.09–0.17	3.91–5.12	4–6	–	5	Fransson (2004)
Sea ice	Bay of Bothnia Baltic Sea	–	–	0.65–1.98	–	321–472	–	(Suominen et al., 2013)
Rafted sea ice block	Beaufort Sea	−11	0.08	1.04–4.04	4.5	–	2–12	(Frederking and Timco, 1983)

Table 4
Ice properties as measured according to ITTC guidelines (2021).

Date and Substructure	Ice Type	T	v_t	σ_i*	σ_c	σ_f	E	h	
[−]	[−]	[°C]	[mm s^{-1}]	[kPa]	[kPa]	[kPa]	[MPa]	[mm]	
06.04.2023 Pile	Cold	−11	0.1	1567	678.1	491.7	3810	25	Fig. 4
12.04.2023 SLS-Print-R	Cold	−11	0.2	1776	709.1	484.3	4152	25	Fig. 7
25.04.2023 SLS-Print-C	Cold	−11	0.1	1656	1054	544.6	5012	25	Fig. 5

* The crushing strength σ_i is based on Eq. 5 in ITTC guidelines (2021), using a contact factor of 0.7 and maximum force measurements during rigid indenter tests, and is given as reference to the compression strength.

dynamic ice-induced vibration regimes in Fig. 6 (one regime per row) shows that scaling effects related to the change in aspect ratio for the two tested diameters (i.e., aspect ratio change from 8 to 12) on the ice-induced vibrations are negligible.

4.2. Shape

The results from rigid indenter tests with two different shapes are depicted in Fig. 7. The use of a rectangular SLS-print or a cylindrical SLS-print did not significantly shift the transition speed or affected the velocity effect. However, the rectangular SLS-print exhibited higher maximum loads when compared to the cylindrical SLS-print with the same nominal area at the ice interface (i.e., 9.7% higher loads for the highest peak loads). This discrepancy in loads is attributed to the greater resistance of ice to move around the rectangular SLS-print, leading to higher confinement and is a common observation (see Table 27 of Korzhavin (1962)).

However, it was observed that low ice drift speeds resulted in radial crack formation when testing the rectangular SLS-print. This crack formation is presumably linked to high stress concentrations at the corners of the SLS-print. The high stress concentration could also explain the chipping of red paint at the corners of the SLS-print during crack formation (refer to Fig. 2).

Investigating the effect of a change in shape and aspect ratio on the development of ice-induced vibrations, dynamic ice-induced vibration experiments of structures with two different aspect ratios and shapes were conducted in the cold model ice. The comparison of time series for three dynamic ice-induced vibration regimes in Fig. 8 (one regime per row) shows that scaling effects related to the change in shape and aspect ratio for the two tested diameters and shapes (i.e., aspect ratio change from 8 to 12; cylindrical to rectangular) on the ice-induced vibrations are negligible. However, it was noted that radial cracks at the corners of the rectangular SLS-print occurred.

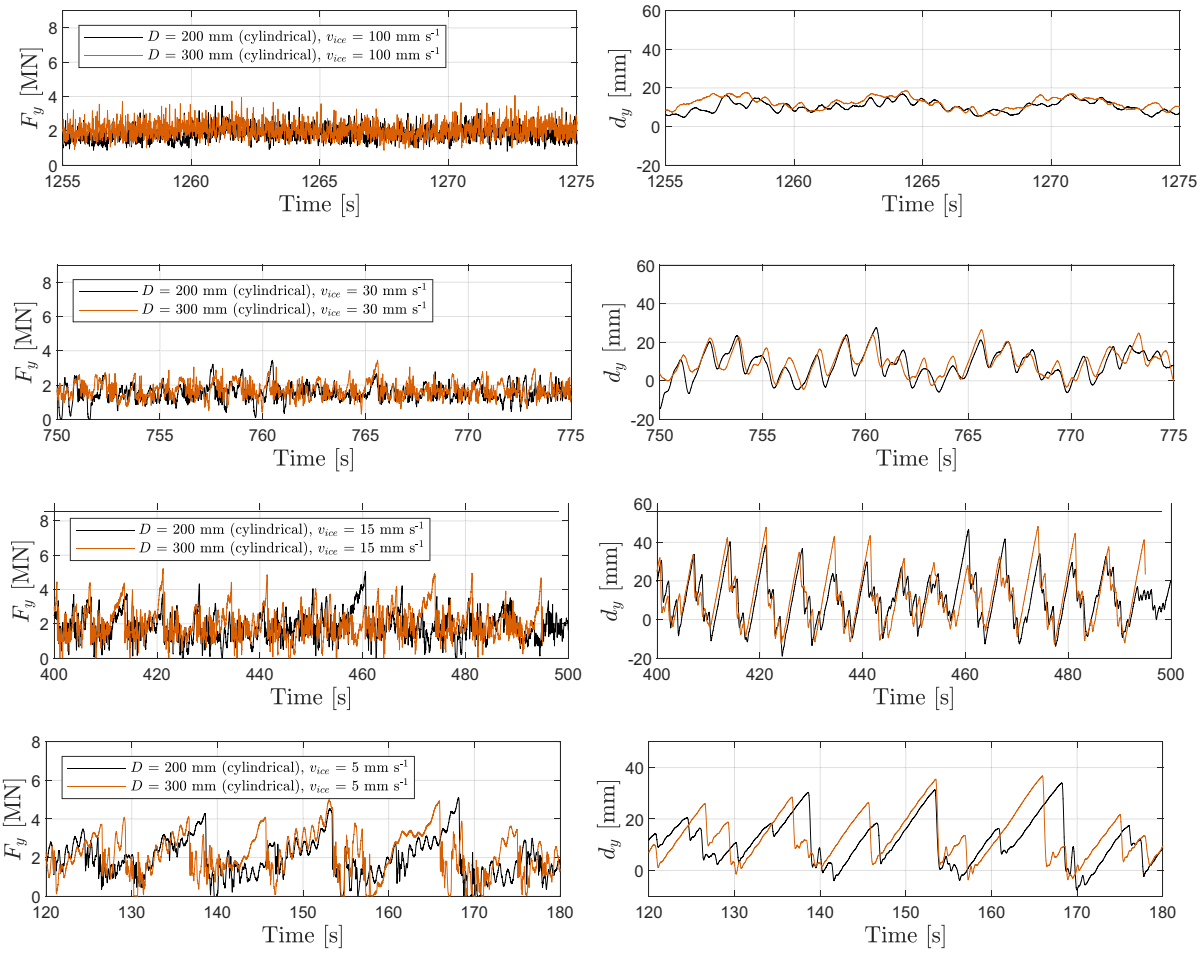

Fig. 6. Time series of dynamic ice-induced vibrations experiments for two structures with different diameter. (Loads at full-scale.)

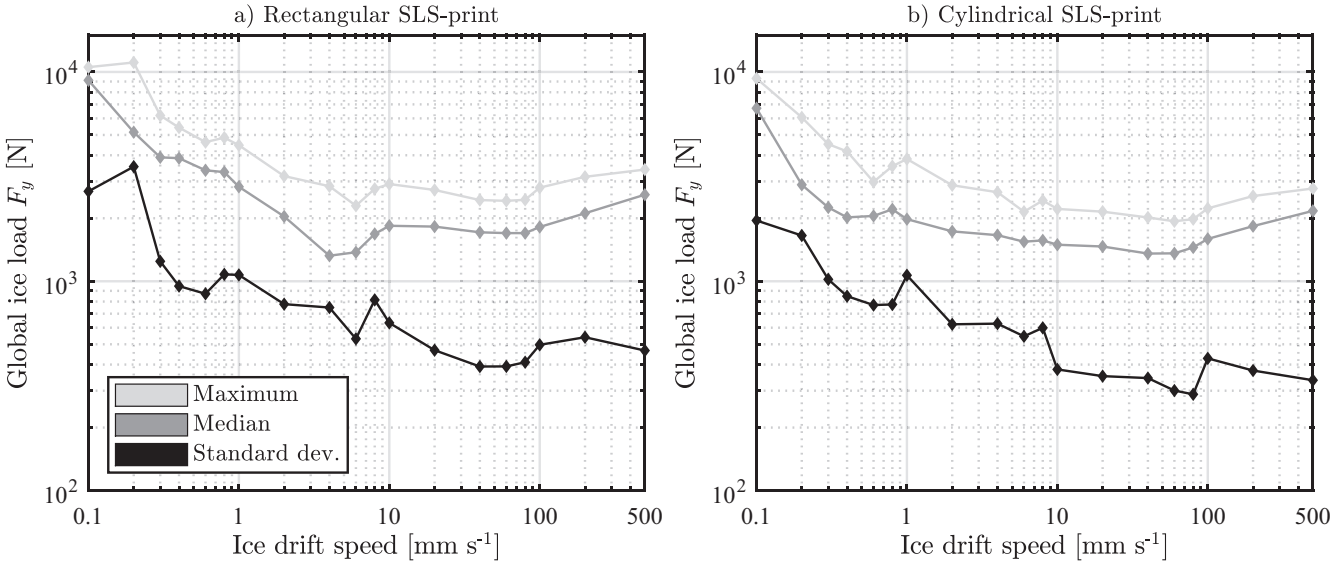

Fig. 7. Results of rigid indenter tests for two different structure shapes with the same effective width.

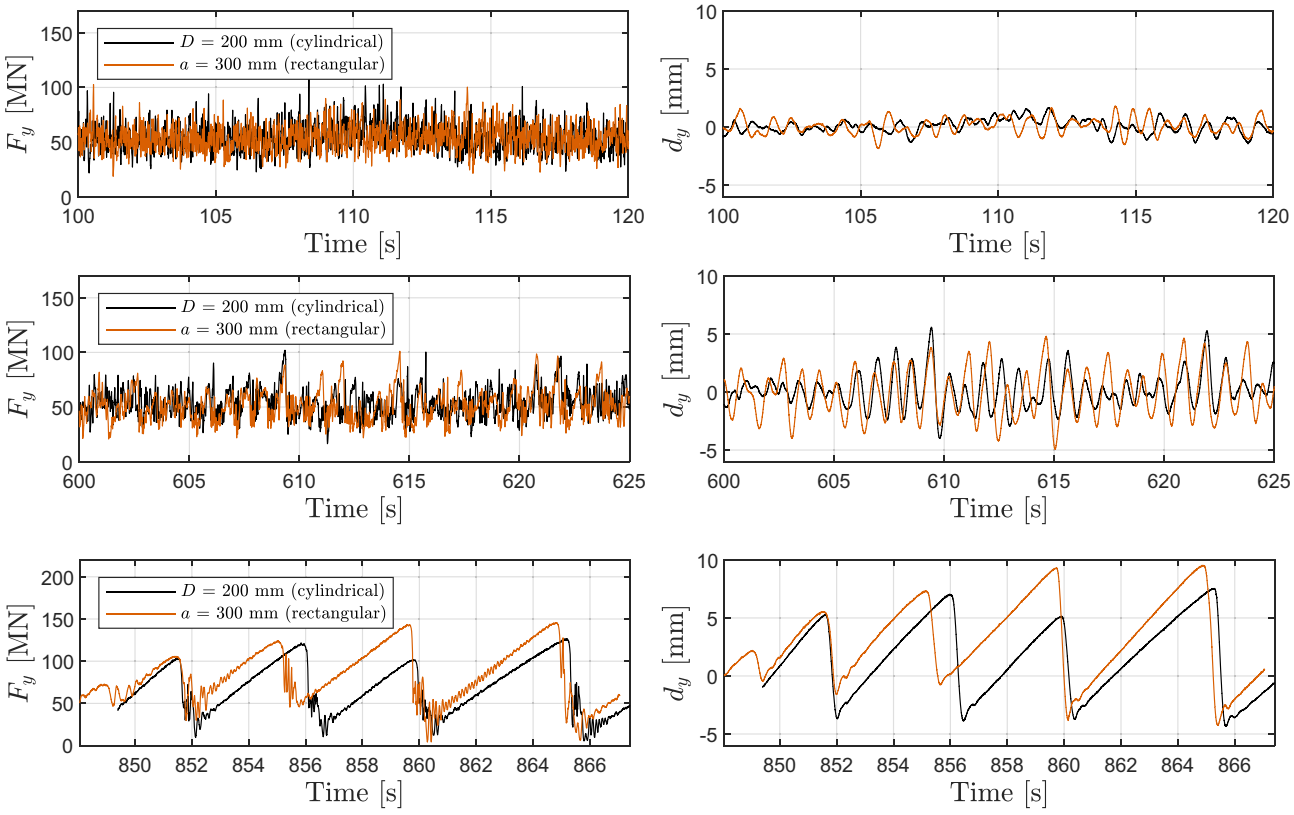

Fig. 8. Time series of dynamic ice-induced vibrations experiments for two structures with different shape and diameter. (Loads at full-scale.)

5. Validation

Finally, the suggested scaling method is applied to investigate if representative ice-induced vibrations of offshore structures can be reproduced by ice tank experiments. Experimental findings are compared to full-scale events. Acknowledging the presence of uncertainties in the environmental data of the full-scale dataset, it is imperative to recognize that this chapter serves the purpose of identifying if the ice-induced regimes can be predicted qualitatively, rather than striving to achieve a quantitative match with the data. However, to generate a qualitative comparison, classification criteria are applied to identify the ice-induced vibration regimes that developed. The criteria established to classify ice-induced vibration regimes R_{IIV} draw upon the classification framework for ice-induced vibrations of offshore wind turbines (Hammer et al., 2022). Thus, intermittent crushing (ICR), multi-modal interaction (MMI), frequency lock-in (FLI), and continuous brittle crushing (CBR) have been categorized through the application of the following formula:

$$R_{IIV} = \begin{cases} \textbf{ICR}, \textbf{if periodicity}^{*} \textbf{ and } T_{peak} < 0.5 \bullet T_{nat,1} \\ \textbf{ICR or FLI if} \textit{periodicity}^{*} \textbf{ and } 0.5 \bullet T_{nat,1} < T_{peak} < CI(1) \bullet T_{nat,1} \\ \textbf{FLI (or MMI), if} \textit{periodicity}^{*} \textbf{ and } CI(1) \bullet T_{nat,i} < T_{peak} < CI(2) \bullet T_{nat,i} \textbf{ and } v_{rel}{}^{**} < v_1 \\ \textbf{CBR}, \textbf{if no apparent} \textit{periodicity}^{*}. \end{cases} \quad (2)$$

* Periodicity of structural response

** When investigating MMI also higher mode vibrations must be checked to distinguish superposed highfrequency oscillations from higher mode lock-in vibrations.

Here T_{peak} is the peak period of structural response (i.e., structural acceleration) as manifested in the measurements, while $T_{nat,i}$ signifies the natural period associated to the mode i of the numerical structure model. A coupling interval (CI) is introduced to incorporate the effects of added mass and damping on the period of vibration (here CI = [0.8, 1.2]). The periodic relative velocity between structure and ice is defined as v_{rel}. The velocity v_1 is the largest ice velocity at which a load peak increase caused by simultaneous ice failure can be measured in rigid indenter experiments.

Ice-induced vibrations as experienced by two full-scale offshore structures were simulated by applying the scaling method introduced in this work: the Norströmsgrund lighthouse (NSG lighthouse) and the Molikpaq platform (Molikpaq).

5.1. Molikpaq event

The Molikpaq platform experienced notable ice-induced vibrations on the 12th of May, 1986, while operating in the Beaufort Sea, as documented by Jefferies and Wright (1988), and analyzed by Gagnon (2012) and Owen and Hendrikse (2021). The full-scale mean brittle crushing ice load from intact ice involved in the dynamic process ($\overline{F}_f$) was estimated as 50 MN. This estimation is based on the load measurement during the Molikpaq event as visualized in Gagnon (2012). As demonstrated by Gagnon, a static baseline load (i.e., ice rubble force) of roughly 100 MN should be subtracted from the total load signal to get an

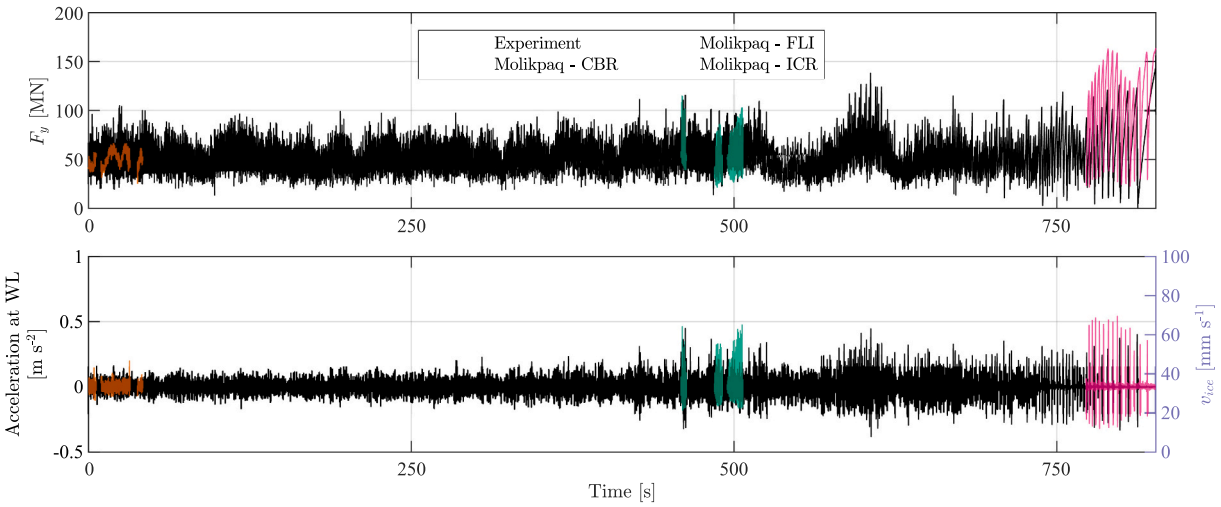

Fig. 9. Experimental results in comparison to ice-induced vibrations of the Molikpaq event on the 12.05.1986.

estimation of the mean brittle crushing ice load. To simulate the ice-induced vibration event of the Molikpaq platform, experiments were conducted using a decelerating "ramped" ice drift speed as also the ice floe during the event slowed down when crushing against the structure. The starting ice drift speed was based on the documented full-scale ice drift speed of 85 mm s^{-1} (Kärnä, 2011b). Given that experiments for the Molikpaq event during the first SHIVER model test campaign showed that ice drift speeds between 85 mm s^{-1} and 55 mm s^{-1} predominantly result in continuous brittle crushing and considering the limitations of crushing length in ice tank experiments, the velocity ramp was initiated at an ice drift speed of 55 mm s^{-1}. During the experiments, the ice decelerated at a constant rate of approximately 0.066 mm s^{-2}. The acceleration in full-scale was non-linear which could not be captured in the ice tank. Therefore, it was settled on an estimate for the deceleration around where ICR happened (last minute of the full-scale signal (see Gagnon, 2012)), understanding that this would lengthen the periods of CBR and FLI in the signal (if occurring) compared to full-scale. Although the ice mainly crushed against the flat north side of the Molikpaq platform, a cylindrical structure was used during the experiments to avoid that radial cracks, which are unknown to be representative of those in full-scale, influence the experiments.

The time series of the experiments were low-pass filtered with a cut-off frequency of 5 Hz and 50 Hz for the acceleration and ice load, respectively. The cut-off frequency for the acceleration was chosen with respect to the highest structural frequency considered in numerical structure modeling. After filtering, data have been resampled to the original sampling rate of 50 Hz to improve comparability between time series of the model-scale and full-scale measurements. The full time series of the postprocessed global ice load F_y and structural acceleration at waterline (WL) for the Molikpaq event are shown in Fig. 9 to Fig. 12.

The experimental results of the 'deceleration test,' involving ice drifting against the Molikpaq and here slowing down against the aluminum pile, are compared in Fig. 9 to three burst files included in the full-scale data. It should be noted that the CBR and FLI data, originally presented as a single CBR burst by Kärnä (2011a), have been separated. When zooming in on the three distinct regimes (Fig. 10 for CBR, Fig. 11 for FLI, and Fig. 12 for ICR), it can be shown that all regimes have been representatively reproduced. The overprediction in the standard deviation of the ice load during continuous brittle crushing is assumed to be caused by the upscaling of non-simultaneous failure peaks (see section 4.1). Also, response periods simulated in the experiments are slightly longer than in full-scale as the ice floe deceleration was underestimated.

5.2. Norströmsgrund (NSG) lighthouse events

The NSG lighthouse is situated in the Bothnian Bay, located in the Northern Baltic Sea. Full-scale measurements of ice loads and structural acceleration for the lighthouse were conducted during the STRICE test campaign between 2000 and 2003 (Kärnä and Jochmann, 2003). Post-processed data from the ice-induced vibration events on the 4th of April 2002, 25th of March 2003, and 9th of April 2001 were analyzed in the ice-induced vibrations Joint Industry Project (Kärnä, 2011a). For validation purposes, ice loads and accelerations recorded during these events were used in the present study. The full-scale mean brittle crushing ice loads ($\overline{F_f}$) of 0.377 MN, 1.559 MN and 1.011 MN, along with constant ice drift speeds (v_{ice}) of 30 mm s^{-1}, 50 mm s^{-1} and 100 mm s^{-1}, respectively, were extracted from the project report. Due to uncertainty in full-scale ice drift speed measurements (Kärnä, 2011a), experiments were conducted with ice drift speeds at, above, and below the full-scale ice drift speeds observed. Tests for the NSG lighthouse were performed exclusively with the aluminum pile.

The time series of the experiments were low-pass filtered with a cut-

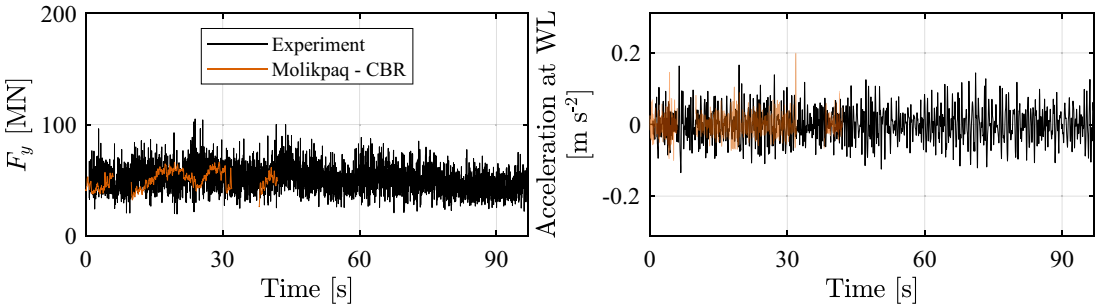

Fig. 10. Comparison of experimental results and full-scale data of the Molikpaq event on the 12.05.1986 at high ice drift speed (continuous brittle crushing).

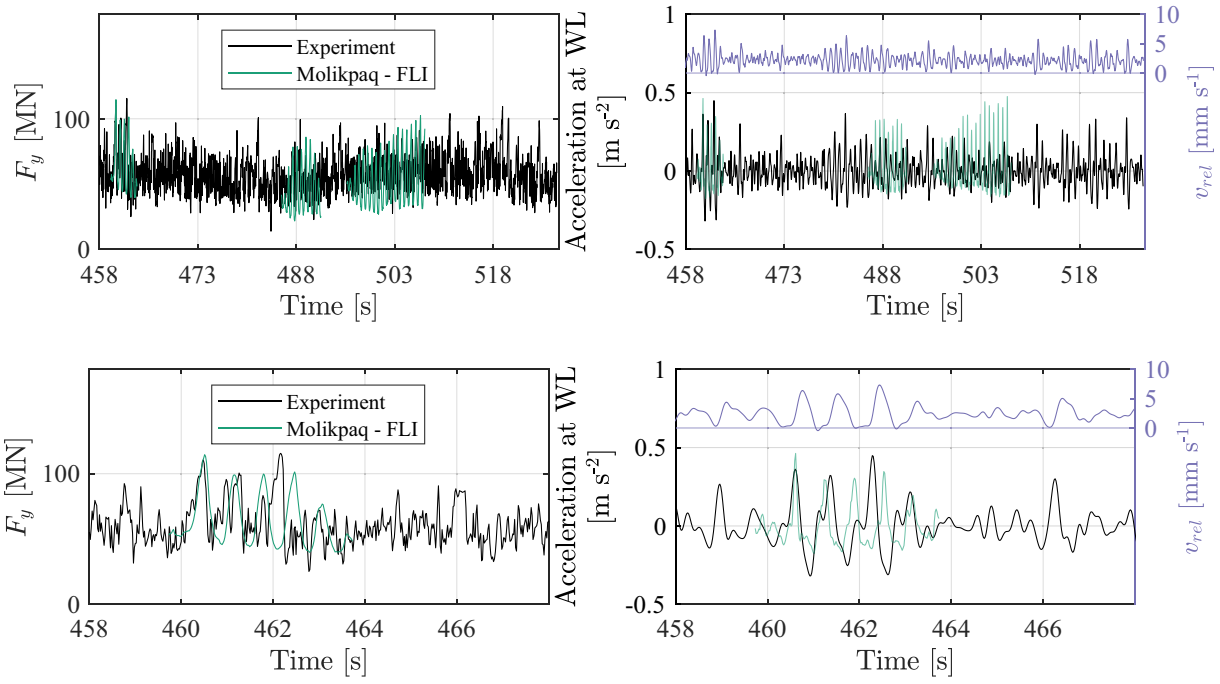

Fig. 11. Top row: Comparison of experimental results and full-scale data of the Molikpaq event on the 12.05.1986 at intermediate ice drift speed (bursts of amplified load and response representative for frequency lock-in). Bottom row: Close-up.

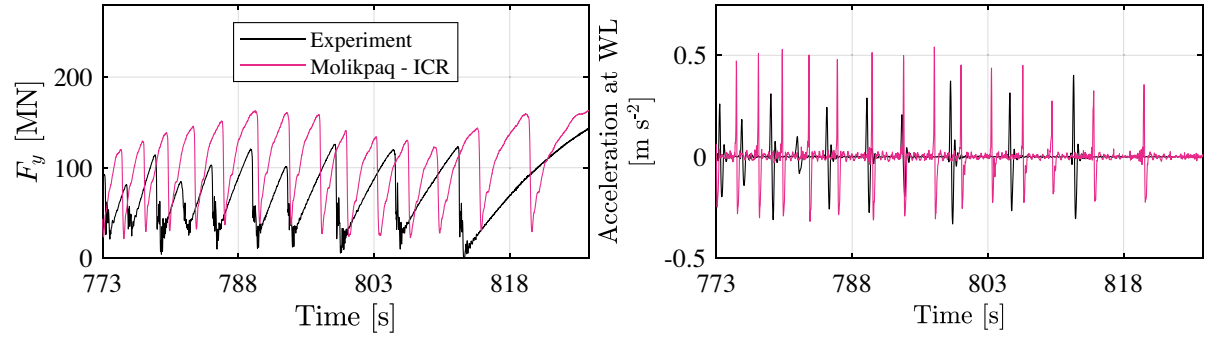

Fig. 12. Comparison of experimental results and full-scale data of the Molikpaq event on the 12.05.1986 at low ice drift speed (intermittent crushing).

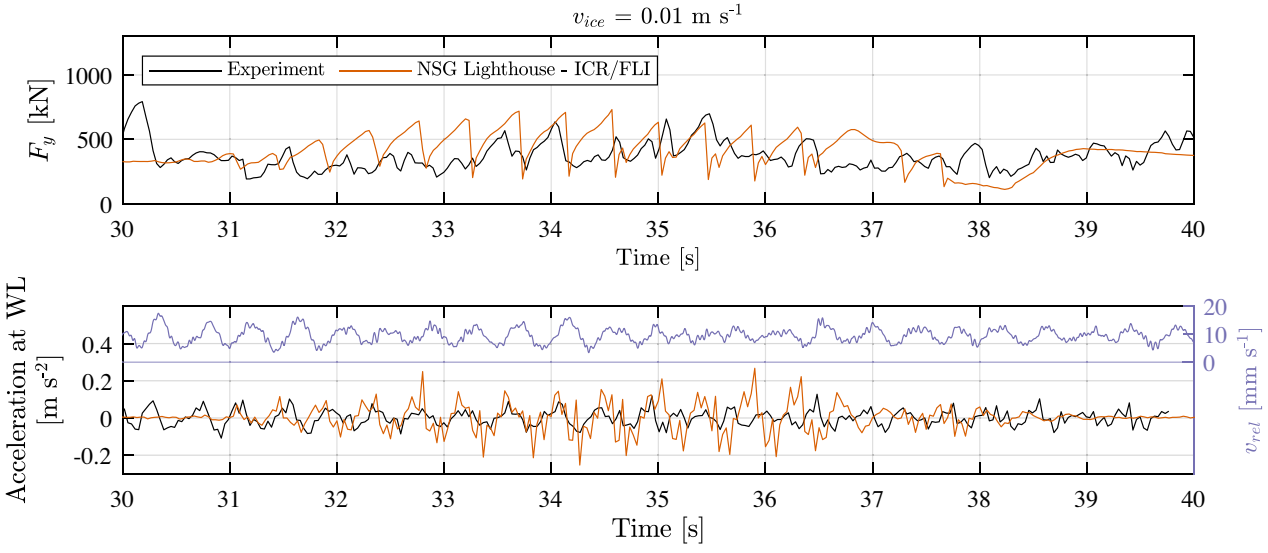

Fig. 13. Experimental results in comparison to the IIV-event of the NSG lighthouse on the 04.04.2002.

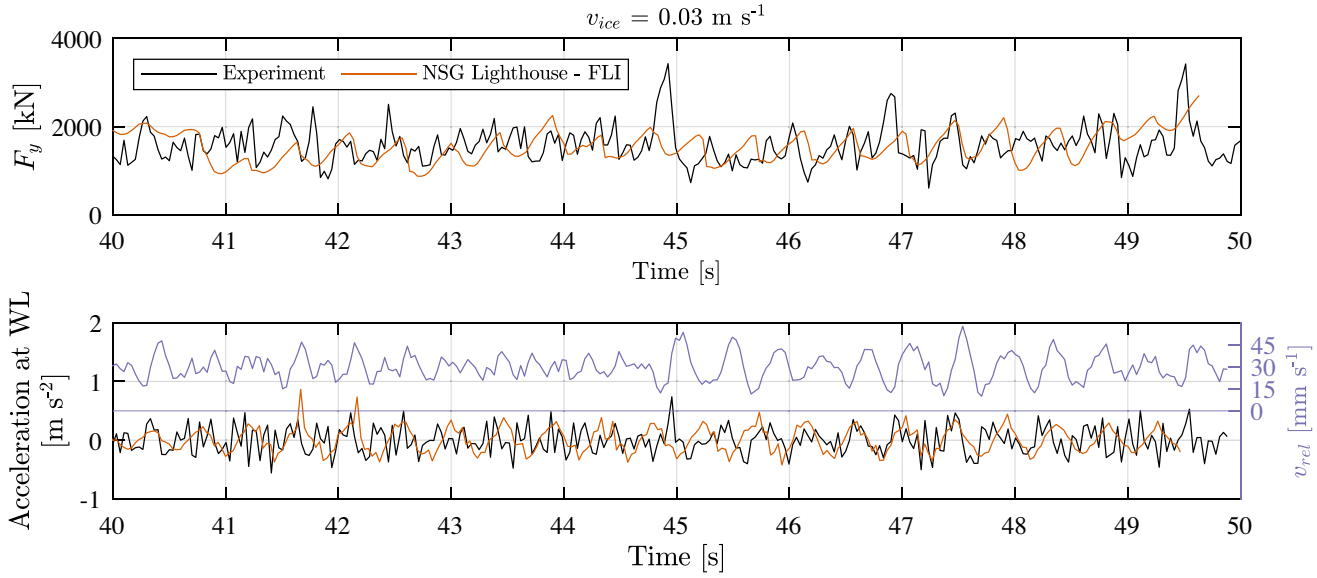

Fig. 14. Experimental results in comparison to the IIV-event of the NSG lighthouse on the 25.03.2003.

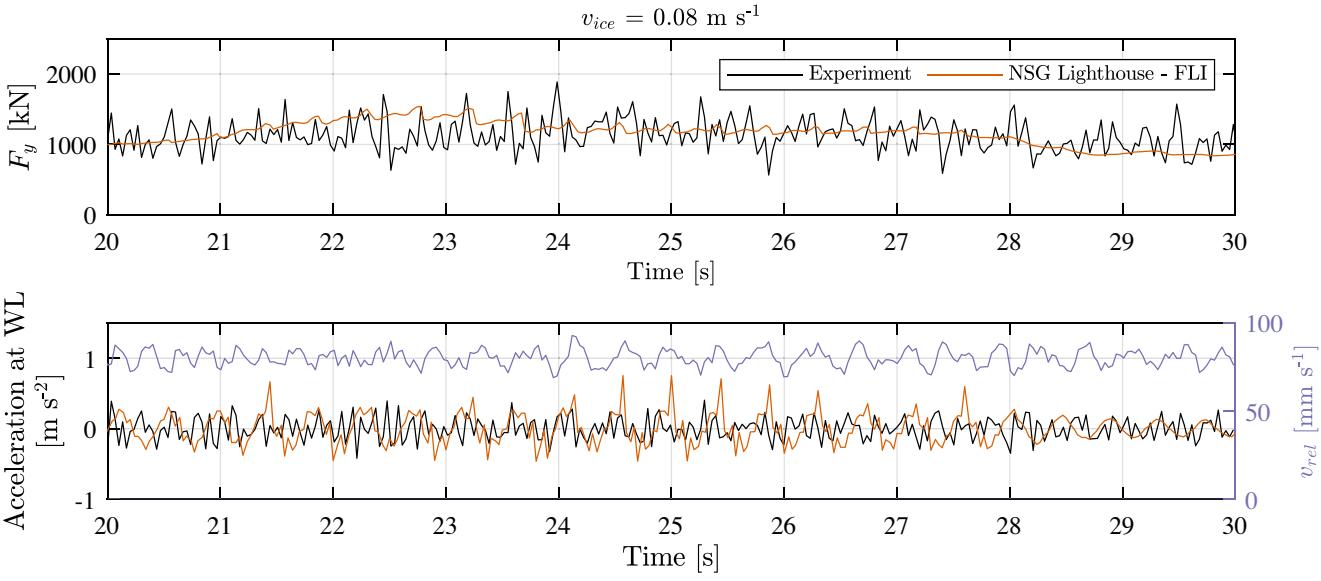

Fig. 15. Experimental results in comparison to IIV-event of the NSG lighthouse on the 09.04.2001.

Table 5
Summary of validation cases.

Event Date	Regimes based on Kärnä (2011a)	v_{ice} [mm s^{-1}]	R_{IIV}	v_{ice} [mm s^{-1}]	
	Molikpaq				
12.05.1986	CBR	>85	CBR	>30	Fig. 10
12.05.1986	"Phase locked"	85>v_{ice}<10	FLI	30>v_{ice}<10	Fig. 11
12.05.1986	ICR	<10	ICR	<10	Fig. 12
	NSG lighthouse				
04.04.2002	ICR/FLI	30	FLI/ CBR	10	Fig. 13
25.03.2003	FLI	50	FLI/ CBR	30	Fig. 14
09.04.2001	FLI	100	CBR	80	Fig. 15

off frequency of 30 Hz for both acceleration and ice load of the NSG lighthouse. The cut-off frequency for the acceleration was chosen with respect to the highest structural frequency considered in numerical structure modeling. After filtering, data have been resampled to the original sampling rate of 30 Hz to improve comparability between time series of the model-scale and full-scale measurements. The full time series of the postprocessed global ice load F_y and structural acceleration at waterline (WL) are shown in Fig. 13 to Fig. 15.

Focusing on the experimental results for the ice-induced vibration event of the NSG lighthouse on the 04.04.2002 in Fig. 13, tendencies towards frequency lock-in can be found. However, those vibrations are not as pronounced as observed in full-scale.

Experimental results for the ice-induced vibration event of the NSG lighthouse on the 25.03.2003 in Fig. 14 show a short lock-in burst starting at $t = 45$ s, which is also visible by the higher load peaks in the load signal. Neither vibrations of the NSG lighthouse in full-scale nor vibrations as measured in experiments were sustained.

Experimental results in Fig. 15 cannot be validated as no tendency to

frequency lock-in occurred. This finding is discussed in Chapter 5.

A summary of the experimental results for the Molikpaq platform and NSG lighthouse is provided in Table 5. The experiments managed to successfully reproduce the regimes of ice-induced vibrations observed in full-scale (i.e., ICR, FLI/MMI, and CBR) except for frequency lock-in event on 09.04.2001. The primary difference observed between the model-scale experiments and full-scale events was that the NSG lighthouse frequency lock-in events could only be converged to at lower ice drift speeds compared to those documented in the full-scale events (Fig. 5).

The selected events were chosen as these were seen as most representative full-scale events of ice-induced vibrations at the time of execution of the JIP. Additional details of the experiments conducted for the Molikpaq and the NSG lighthouse can be found in Table 1 and Table 2 in the supplementary material including corresponding velocity profiles and implemented dynamic structural models. Note that the structural properties in the structural files, which also can be found in the supplementary material, were scaled for the measured mean ice load ($\bar{F}_m$) during the experiments. A summary of the full-scale events can be found in Kärnä et al. (2013), from which the table of selected validation cases was reproduced in Table 3 in the supplementary material.

6. Discussion

6.1. Scaling verification

The present study aimed to verify our proposed modeling technique for the application of ice-structure interaction of vertically sided structures. The cold model ice failed purely in crushing and produced a load increase at lower ice drift speeds (velocity effect). Other types of model ice, such as the 'wave model ice' developed by Ziemer (2021), also have been shown to fail in crushing. If these model types can demonstrate a velocity effect and transition speeds comparable to sea ice, they could potentially be utilized for applying the present scaling method.

The verification of the transition speed is subject to uncertainty as transition speeds in sea ice were determined via uniaxial compression tests, while rigid indenter experiments were performed with floating model ice. While it was decided to preserve the transition speed from ductile-to-brittle crushing, it is likely that this parameter is controlled by a more fundamental ice property, for example the ice temperature.

During the verification process, the requirement for elastic and strength similarity was relaxed. This decision was based on the understanding that achieving similar elasticity and strength in ice might not be essential when attempting to reproduce ice-induced vibrations. As

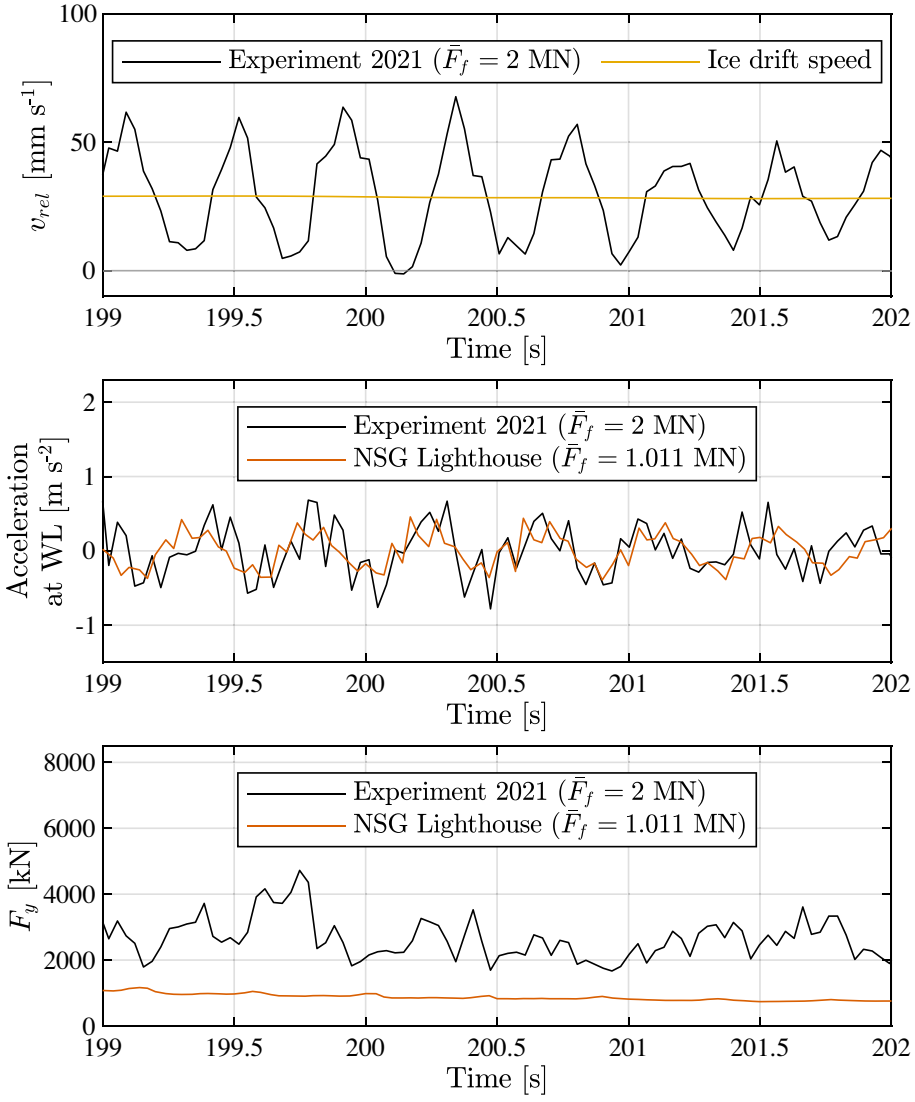

Fig. 16. Measurements of the experiments of the first SHIVER model test campaign for the NSG lighthouse scaled with $\bar{F}_f = 2$ MN in comparison to recordings during the full-scale event on 09.04.2001.

the present study managed to reproduce full-scale experiments while relaxing the elastic and strength similarity, this approach seems to be reasonable.

Results indicated that no significant aspect ratio effect occurred in the experiments. Nonetheless, the difference between the investigated physical substructures diameter was small (aspect ratio change from 8 to 12). Experiments with a larger diameter are expected to manifest scaling effects in the magnitude of standard deviation due to averaging of high-pressure zone formation for a larger area. This scaling effect could explain the different magnitude of the standard deviation of ice loads during continuous brittle crushing of the Molikpaq platform (see Fig. 10, left). However, representative ice-induced vibrations can still be achieved as the scaling method is based on the mean ice load level and not on peak pressures.

The rectangular print led to the formation of radial cracks during testing. However, no further analysis regarding crack frequency, formation, propagation, or their representativeness for ice-induced vibrations of the Molikpaq platform was performed, as the cylindrical pile already yielded representative outcomes.

6.2. Validation

While the model-scale results for the Molikpaq structure were relatively good in terms of the different ice-induced vibration regimes observed during the slowing down of an ice floe, the results for the Norströmsgrund lighthouse require some further discussion.

Frequency lock-in of the NSG lighthouse model for environmental conditions applied as documented for the 9th of April, 2001 was not observed in the ice tank. A challenge here is that the NSG lighthouse as a relatively stiff structure almost never experienced long sustained frequency lock-in events, as for example observed for the more flexible structures in the Bohai Bay (Yue et al., 2002). Given the non-linearity of the ice-structure interaction, the initial conditions play a significant role in cases where sustained lock-in is not possible. As seen during the experiment simulating the event on the 25th of March (Fig. 14), the tendency to frequency lock-in only occurred for part of the time. This is very representative of the full-scale scenario, but also shows how difficult it is to use these full-scale data for validation as one cannot generate specific initial conditions in an ice tank. Such initial conditions have been reported upon by Bjerkås (2006), for example, as smooth ice edges interacting with the lighthouse because of previous radial cracking.

When the full-scale reference ice load was increased to 2 MN in the previous model test campaign, it was found that frequency lock-in of the NSG lighthouse does occur in the cold model ice (Fig. 16). This is indicative that the experiments conducted are at the boundary between no frequency lock-in and sustained frequency lock-in which corresponds well to the actual full-scale observations. We note that it is no challenge to obtain sustained lock-in signals in an ice tank, the challenge is to end up in the boundary regime where the ice load magnitude is just insufficient for sustained frequency lock-in, but in certain cases of specific initial conditions (high peak load, slightly thicker than average ice) can trigger short bursts of vibrations.

Notably, there is some uncertainty with respect to the full-scale load levels due to only partial instrumentation of the waterline of the NSG lighthouse with load panels. In addition, recordings of a camera attached to the structure were used to define the ice drift speeds. The authors of the report themselves acknowledged the potential for an overestimation of the documented ice drift speeds (Kärnä, 2011a). Testing for too high ice drift speeds promotes continuous brittle crushing over frequency lock-in.

6.3. Data reliability

To assess the reliability of the data, a comparison between median ice loads obtained from a direct shear load measurement and the identified, horizontal ice loads was conducted in the present study. The comparison results are presented in Figure 1 in the supplementary material, revealing a good agreement between the two measurements. Within the same figure, vertical loads appear minor in contrast to horizontal loads. Consequently, it is assumed that no significant upward or downward ice movement occurred. This observation is corroborated by the paint removal on the prints (refer to Fig. 2), indicating that the model ice exerted force against the structure at the anticipated interaction point mainly.

The shortening of the aluminum pile and the utilization of honeycombed SLS-prints minimized masses affecting load cell measurements. The contribution of inertial loading was thus negligible.

6.4. Application

Further, the applicability of the suggested scaling method is contingent upon the quality of the environmental load envelope (same holds for numerical simulations). Once these conditions are known, the full-scale mean (or alternatively, median) brittle crushing ice load can for example be estimated utilizing eq. A.8–21 of ISO 19906 (2019). Alternatively, the value can be extracted from an ice model simulation during continuous brittle crushing with a rigid structure. An application of the suggested scaling method for offshore wind turbines for which no full-scale data yet exists can be found in the study by Hammer et al. (2023).

Finally, it is emphasized that the scaling method was exclusively applied for two full-scale structures. Comprehensive and synchronized high-resolution measurements of ice load and structural displacement of an offshore structure facing crushing ice loads, along with synchronized environmental data (e.g., ice drift speed measurements), would be invaluable for further evaluation of the proposed scaling method. This limitation constitutes the most significant constraint of the present study.

6.5. Limitations

The investigated scaling method can be applied to offshore structures subjected to predominantly crushing ice loads. As highlighted in the introduction, other dominant failure modes would likely not allow to neglect global mass similarity. Also at higher ice drift speeds, ice extrusion prevents the neglection of mass similarity. The scaling method is thus only valid when the mean ice load used for scaling is rate-unaffected (see Fig. 3).

The scaling approach is not focusing on local peak pressures or exact peak loads during high-speed crushing. Thus, it is not critical that the aspect ratio scale effect is inhibiting a qualitative reproduction of the high frequency peaks during continuous brittle crushing.

Another limitation of the study is the requirement of a mean ice load estimation for applying the scaling. However, mean loads can be estimated by ice models coupled to rigid structures, while it is the dynamic ice load that is most critical in design. Additionally, it is crucial to underscore that the approach was verified for structures with relatively low first natural frequencies (0.15–2.5 Hz). Whether structures with higher frequencies can be assessed in a similar manner remains to be tested.

7. Conclusion

The combination of replica modeling and preservation of kinematics during ice-structure interaction has been applied as a modeling technique for investigating ice-induced vibrations of vertically sided offshore structures in ice tank experiments. Based on recent theoretical developments, the kinematics during ice-structure interaction, the transition speed, the velocity effect and the mean brittle crushing load level were chosen to define the energy transfer to the structure and thus controlling the mechanism of ice-induced vibrations.

It has been proposed that the model ice must fail in crushing and

demonstrate both the existence of a transition speed and velocity effect for rigid structures. The transition speed from ductile-to-brittle failure was adopted as a reference property of the ice, defining its time- and rate-dependent behavior. The ratio of the full-scale to the model-scale mean brittle crushing ice load was used to scale numerical structure properties to preserve kinematics during real-time hybrid simulations in model ice.

Thorough rigid indenter experiments in combination with ice-induced vibrations experiments of structures with different aspect ratio and shape were conducted to verify the scaling approach. No observable scaling effects on the velocity effect, transition speed, and development of ice-induced vibrations were found when varying between a cylindrical and rectangular shape, or when changing the aspect ratio in a range between 8 and 12.

The proposed scaling technique was qualitatively validated by performing novel ice tank experiments to reproduce the full-scale ice-induced vibrations experienced by the Molikpaq platform and the Norströmsgrund lighthouse.

Regrettably, the lack of well-documented, synchronized, and high-frequency sampled full-scale measurements on structures susceptible to ice-induced vibrations continues to hinder a quantitative validation of scaling approaches, though the results obtained in the experiments are promising.

Author contribution

Tim C. Hammer (Model ice & Scaling & Ice-induced vibrations): Conceptualization, Data curation, Formal analysis, Investigation, Methodology, Project administration, Software, Supervision, Validation, Visualization, Writing – original draft. Otto Puolakka (Model ice): Conceptualization, Methodology, Project administration, Resources, Supervision. Hayo Hendrikse (Model ice & Scaling & Ice-induced vibrations): Conceptualization, Funding acquisition, Investigation, Methodology, Project administration, Supervision, Validation, Writing – review & editing.

Declaration of competing interest

The authors declare that they have no known competing financial interests or personal relationships that could have appeared to influence the work reported in this paper.

Data availability

The experimental data can be obtained from the 4TUResearchData repository (https://doi.org/10.4121/6a696ee6-bed5-48b6-84cd-11385da2ee56.v1).

Acknowledgements

The authors express gratitude to the contributing organizations of the SHIVER project: TU Delft and Siemens Gamesa Renewable Energy, whose support was instrumental in this endeavor. The SHIVER project is co-financed by Siemens Gamesa Renewable Energy and TKI-Energy through the 'Toeslag voor Topconsortia voor Kennis en Innovatie (TKI's)' initiative of the Dutch Ministry of Economic Affairs and Climate Policy. Special recognition is extended to Teemu Päivärinta and Lasse Turja from the Aalto Ice and Wave Tank, and Arttu Polojärvi and Alice Petry from Aalto University School of Engineering, as well as Laura van Dijke and Cody C. Owen from TU Delft, and Jeffrey Hoek from Siemens Gamesa Renewable Energy, who provided invaluable assistance during the model test campaign. Additional credits are given to Cody C. Owen for commenting on the manuscript.

This work was made possible through the financial support of TKI-Energy via the 'Toeslag voor Topconsortia voor Kennis en Innovatie (TKI's)' initiative of the Dutch Ministry of Economic Affairs and Climate Policy. (Grant reference: TKITOE_WOZ_1906_TUD_SHIVER.)).

During the preparation of this work the authors used ChatGPT 3.5 in order to improve readability of the text passages. After using this tool/service, the authors reviewed and edited the content as needed and take full responsibility for the content of the publication.

Appendix A. Supplementary data

Supplementary data to this article can be found online at https://doi.org/10.1016/j.coldregions.2024.104127.

References

Baker, W.E., Westine, P.S., Dodge, F.T., 1991. Similarity Methods in Engineering Dynamics, Revised Ed. Elsevier Science Publishers B.V, Amsterdam.

Barker, A., et al., 2005. Ice loading on Danish wind turbines. Part 1: Dynamic model tests. Cold Reg. Sci. Technol. 41 (1), 1–23. https://doi.org/10.1016/j.coldregions.2004.05.002.

Bjerkås, M., 2006. Ice Actions on Offshore Structures with Applications of Continuous Wavelet Transforms on Ice Load Signals. Norwegian University of Science and Technology. Available at: https://ntnuopen.ntnu.no/ntnu-xmlui/handle/11250/231352.

Cole, D.M., 2021. A constitutive model for sea ice: Physical basis, formulations, examples and applications. In: Proceedings of the 26th International Conference on Port and Ocean Engineering under Arctic Conditions. POAC, Moscow, Russia, pp. 1–12. Available at: https://poac.com/Papers/2021/pdf/POAC21-010.pdf.

Cole, D.M., Durell, G.D., 1995. The cyclic loading of saline ice. Philos. Mag. A 72 (1), 209–229. https://doi.org/10.1080/01418619508239591.

Cornett, A.M., Timco, G.W., 1998. Ice loads on an elastic model of the Molikpaq. Appl. Ocean Res. 20 (1–2), 105–118. https://doi.org/10.1016/S0141-1187(98)00006-6.

Fransson, L., 2004. 'Mechanical properties of ice at Norströmsgrund, Tests 2003', Technical Report of the STRICE project, pp. 1–30. Available at: https://www.diva-portal.org/smash/get/diva2:997929/FULLTEXT01.pdf.

Frederking, R., Timco, G., 1983. Uniaxial compressive strength and deformation of Beaufort Sea ice. In: Proceedings of the 7th International Conference on Port and Ocean Engineering under Arctic Conditions. Helsinki, Finland, POAC, pp. 89–98.

Gagnon, R.E., 2012. An explanation for the Molikpaq May 12, 1986 event. Cold Reg. Sci. Technol. 82, 75–93. https://doi.org/10.1016/j.coldregions.2012.05.009.

Gravesen, H., et al., 2005. Ice loading on Danish wind turbines: Part 2. Analyses of dynamic model test results. Cold Reg. Sci. Technol. 41 (1), 25–47. https://doi.org/10.1016/j.coldregions.2004.05.009.

Hammer, T.C., Hendrikse, H., 2023. Experimental study into the effect of wind-ice misalignment on the development of ice-induced vibrations of offshore wind turbines. Eng. Struct. 286, 1–17. https://doi.org/10.1016/j.engstruct.2023.116106.

Hammer, T.C., et al., 2021. A 2D test setup for scaled real-time hybrid tests of dynamic ice- structure interaction. In: Proceedings of the 26th International Conference on Port and Ocean Engineering under Arctic Conditions. Moscow, Russia, POAC, pp. 1–13. Available at: http://resolver.tudelft.nl/uuid:a0b53799-8f0c-4c29-a095-5bd45f5cd56e.

Hammer, T.C., et al., 2022. Classification of ice-induced vibration regimes of offshore wind turbines. In: Proceedings of the ASME 2022 41st International Conference on Ocean, Offshore and Arctic Engineering. Hamburg, Germany, OMAE, pp. 1–8. https://doi.org/10.1115/OMAE2022-78972.

Hammer, T.C., Willems, T., Hendrikse, H., 2023. Dynamic ice loads for offshore wind support structure design. Mar. Struct. 87, 1–19. https://doi.org/10.1016/j.marstruc.2022.103335.

Hendrikse, H., Nord, T.S., 2019. Dynamic response of an offshore structure interacting with an ice floe failing in crushing. Mar. Struct. 65, 271–290. https://doi.org/10.1016/j.marstruc.2019.01.012.

Hendrikse, H., Ziemer, G., Owen, C.C., 2018. Experimental validation of a model for prediction of dynamic ice-structure interaction. Cold Reg. Sci. Technol. 151, 345–358. https://doi.org/10.1016/j.coldregions.2018.04.003.

Hendrikse, H., et al., 2022. Experimental data from ice basin tests with vertically sided cylindrical structures. Data Brief 41, 1–18. https://doi.org/10.1016/j.dib.2022.107877.

Hirayama, K., Schwarz, J., Wu, H.-C., 1974. An Investigation of Ice Forces on Vertical Structures. Iowa City, Iowa, USA.

Huang, Y., Shi, Q., Song, A., 2007. Model test study of the interaction between ice and a compliant vertical narrow structure. Cold Reg. Sci. Technol. 49, 151–160. https://doi.org/10.1016/j.coldregions.2007.01.004.

ISO19906:2019(E) Petroleum and natural gas industries — Arctic offshore structures, Issue Second edition, 19906, 2019. ISO, pp. 1–560.

ITTC, 2021. Recommended procedures and guidelines - test methods for model ice properties. In: International towing tank conference, pp. 1–19. Available at: https://www.ittc.info/media/9659/75-02-04-02.pdf.

Izumiyama, K., Irani, M.B., Timco, G.W., 1994. Influence of compliance of structure on ice load. In: Proceedings of the 12th IAHR International Symposium on Ice. Trondheim, Norway, IAHR, pp. 229–238.

Jefferies, M.G., Wright, W.H., 1988. Dynamic response of Molikpaq to ice-structure interaction. In: Proceedings of the 7th International Conference on Offshore Mechanics and Arctic Engineering, Houston, Texas, USA, OMAE,, pp. 201–220.

Jefferies, M., Kärnä, T., Løset, S., 2008. Field data on the magnification of ice loads on vertical structures. In: Proceedings of the 19th IAHR International Symposium on Ice. Vancouver, British Columbia, Canada, IAHR, pp. 1325–1343.
Kamesaki, K., Yamauchi, Y., Kärnä, T., 1996. Ice force as a function of structural compliance. In: Proceedings of the 13th IAHR International Symposium on Ice. Beijing, China, IAHR, pp. 395–402.
Kärnä, T., 2011a. Full-Scale Data Analyses of Frequency Lock-in. Technical Report of the Ice-Induced vibrations JIP project.
Kärnä, T., 2011b. Validation of Predictive IIV HM-Model. Technical Report of the Ice-Induced vibrations JIP project.
Kärnä, T., Jochmann, P., 2003. Field observations on ice failure modes. In: Proceedings of the 17th International Conference on Port and Ocean Engineering under Arctic Conditions. Trondheim, Norway: POAC.. Available at: http://virtual.vtt.fi/virtual/proj6/arki/julkaisut/strice/ObservedFailure Modes_POAC03.pdf.
Kärnä, T., Muhonen, A., 1990. Preliminary results from ice indentation tests using flexible and rigid indentors. In: Proceedings of the 10th IAHR International Symposium on Ice. Espoo/Helsinki, Finland, IAHR, pp. 261–275.
Kärnä, T., et al., 2003. Ice Action on Compliant Structures. Laboratory indentation tests. VTT Research Notes, Espoo, Finland. Available at: https://cris.vtt.fi/en/publications/ice-action-on-compliant-structures-laboratory-indentation-tests.
Kärnä, T., et al., 2008. Small-scale data on magnification of ice loads on vertical structures. In: Jasek, M. (Ed.), Proceedings of the 19th IAHR International Symposium on Ice. IAHR, Vancouver, British Columbia, Canada, pp. 1313–1324.
Kärnä, T., et al., 2013. Ice-induced vibrations of offshore structures - looking beyond ISO 19906. In: Proceedings of the 22nd International Conference on Port and Ocean Engineering under Arctic Conditions. Espoo, Finland, POAC, pp. 1–12.
Korzhavin, K.N., 1962. Action of Ice on Engineering Structures. Publishing House of Siberian Branch of USSR Academy of Sciences.
Määttänen, M., 1978. On Conditions for the Rise of Self-Excited Autonomous Oscillations in Slender Marine Piles, Winter Navigation Reseach Board. University of Oulu.
Määttänen, M., 1979. Laboratory tests for dynamic ice-structure interaction. In: Proceedings of the 5th Port and Ocean Engineering under Arctic Conditions. Trondheim, Norway, POAC, pp. 1139–1153.
Määttänen, M., 1981. Laboratory tests for dynamic ice-structure interaction. Eng. Struct. 3, 111–116. https://doi.org/10.1016/0141-0296(81)90037-7.
Määttänen, M., et al., 2012. Novel ice induced vibration testing in a large-scale facility: Deciphering ice induced vibrations, part 1. In: Proceedings of the 21st IAHR International Symposium on Ice. Dalian, China, IAHR, pp. 946–958.
McCrum, D.P., Williams, M.S., 2016. An overview of seismic hybrid testing of engineering structures. Eng. Struct. 118, 240–261. https://doi.org/10.1016/j.engstruct.2016.03.039.
Owen, C.C., Hendrikse, H., 2021. Simulation and analysis of ice-induced vibrations experienced by Molikpaq during the May 12, 1986 event. In: Proceedings of the 26th International Conference on Port and Ocean Engineering under Arctic Conditions. POAC, Moscow, Russia. Available at: http://resolver.tudelft.nl/uuid:aa680c32-6424-4380-b90c-afcec0bd02ef.
Owen, C.C., Hammer, T.C., Hendrikse, H., 2023. Hysteresis and dichotomous mechanics in cyclic crushing failure of confined freshwater columnar ice. Cold Reg. Sci. Technol. 209, 1–18. https://doi.org/10.1016/j.coldregions.2023.103816.
Petry, A., et al., 2023. Ice basin experiments on mixed-mode failure on ice cones. In: Proceedings of the 27th International Conference on Port and Ocean Engineering under Arctic Conditions. POAC, Glasgow, UK. Available at: http://resolver.tudelft.nl/uuid:25de4d69-44fa-45bd-9b34-ebad2f280046.
Peyton, H.R., 1968. Sea ice forces. In: Proceedings of Conference on Ice Pressures Against Structures, pp. 117–123.
Singh, S.K., et al., 1990. Tests of ice crushing on a flexible structure. In: Proceedings of the 9th Offshore Mechanics and Arctic Engineering Symposium. OMAE, Houston, Texas, USA, pp. 89–94.
Sodhi, D.S., 1991. Ice-structure interaction during indentation tests. In: Jones, S., et al. (Eds.), Proceedings of the IUTAM-IAHR Symposium on Ice-structure Interaction. St. John's, Newfoundland, Canada: Springer-Verlag Berlin Heidelberg, pp. 619–640. https://doi.org/10.1007/978-3-642-84100-2_31.
Sodhi, D.S., 1992. Ice-structure interaction with segmented indentors. In: Proceedings of the 11th IAHR International Symposium on Ice. Banff, Alberta, Canada, IAHR, pp. 909–929.
Sodhi, D.S., 2001. Crushing failure during ice-structure interaction. Eng. Fract. Mech. 68 (17–18), 1889–1921. https://doi.org/10.1016/S0013-7944(01)00038-8.
Suominen, M., et al., 2013. Full-scale measurements on board PSRV S.A. Agulhas II in the Baltic Sea. In: Proceedings of the 22nd International Conference on Port and Ocean Engineering under Arctic Conditions. Espoo, Finland, POAC, pp. 1–13.
Takeuchi, T., et al., 2001. On the factors influencing the scaling of ice forces. In: Dempsey, J.P., Shen, H.H. (Eds.), Proceedings of the IUTAM Symposium on Scaling Laws in Ice Mechanics and Ice Dynamics. Fairbanks, Alaska, USA, IUTAM, pp. 149–160. https://doi.org/10.1007/978-94-015-9735-7_13.
Tian, Y., Huang, Y., Li, W., 2019. Experimental Investigations on Ice Induced Vibrations of a Monopile-type Offshore Wind Turbine in Bohai Sea. In: Proceedings of the 29th International Ocean and Polar Engineering Conference. Honolulu, Hawaii, USA, ISOPE, pp. 327–334.
Timco, G.W., et al., 1992. Model tests of dynamic ice loading on the Chinese JZ-20-2 jacket platform. Can. J. Civ. Eng. 19, 819–832. https://doi.org/10.1139/l92-093#.Xd6NRPlKhPY.
Toyama, Y., et al., 1983. Model tests on ice-induced self-excited vibration of cylindrical structures. In: Proceedings of the 7th International Conference on Port and Ocean Engineering under Arctic Conditions. Helsinki, Finland, POAC, pp. 834–844.
Tsuchiya, M., et al., 1985. An experimental study on ice-structure interaction. In: Proceedings of the 7th Offshore Technology Conference. Offshore Technology Conference, Houston, Texas, USA, pp. 312–327. https://doi.org/10.4043/5055-MS.
von Bock und Polach, R.U.F., Ehlers, S., 2015. On the scalability of model- scale ice experiments. J. Offshore Mech. Arctic Eng. 137, 1–8. https://doi.org/10.1115/1.4031114.
von Bock und Polach, R.U.F., Molyneux, D., 2017. Model ice: A review of its capacity and identification of knowledge gaps. In: Proceedings of the 36th International Conference on Offshore Mechanics and Arctic Engineering. Tondheim, Norway, OMAE, pp. 1–10. https://doi.org/10.1115/OMAE2017-61808.
von Bock und Polach, R.U.F., Ehlers, S., Kujala, P., 2013. Model-scale ice - Part A: Experiments. Cold Reg. Sci. Technol. 94, 74–81. https://doi.org/10.1016/j.coldregions.2013.07.001.
Wei, M., et al., 2022. Response of dry and floating saline ice to cyclic compression. Geophys. Res. Lett. 49, 1–10. https://doi.org/10.1029/2022GL099457.
Wu, H.C., Chang, K.J., Schwarz, J., 1976. Fracture in the compression of columnar gained ice. Eng. Fract. Mech. 8 (2), 365–370. https://doi.org/10.1016/0013-7944(76)90016-3.
Yap, K.T., 2011. Level Ice-Vertical Structure Interaction: Steady-State Self-Excited Vibration of Structures. National University of Singapore. Available at: https://scholarbank.nus.edu.sg/handle/10635/43422.
Yue, Q., et al., 2002. Dynamic ice forces caused by crushing failure. In: Squire, V., Langhorne, P. (Eds.), Proceedings of the 16th IAHR International Symposium on Ice. Dunedin, New Zealand, IAHR, pp. 231–237.
Yue, Q., Guo, F., Chu, S., 2006. Laboratory tests of ice induced structure vibrations. In: Proceedings of the 18th IAHR International Symposium on Ice. Sapporo, Japan, IAHR, pp. 191–198.
Ziemer, G., 2021. Ice-Induced Vibrations of Vertical Structures, Doctoral thesis. Technische Universität Hamburg. https://doi.org/10.15480/882.4018.